Electronic Supplementary Information

Synthesis of Hierarchically Structured ZnO Nanomaterials via Supercritical Assisted Solvothermal Process

Meng Wang [a], *Bin Zhao* [b,] *, *Shaohong Xu* [b], *Lin Lin* [b], *Sijun Liu* [b], *Dannong He* [a, b,] *

[a] School of Materials Science and Engineering, Shanghai JiaoTong University, 800 Dongchuan Road, Shanghai 200240, China.

[b] National Engineering Research Center for Nanotechnology, 28 East Jiangchuan Road, Shanghai 200241, China.

* Corresponding authors. E-mail: zhaobinwily@hotmail.com; dannonghe@126.com. Tel.: +86-21-34291286. Fax: +86-21-34291125.

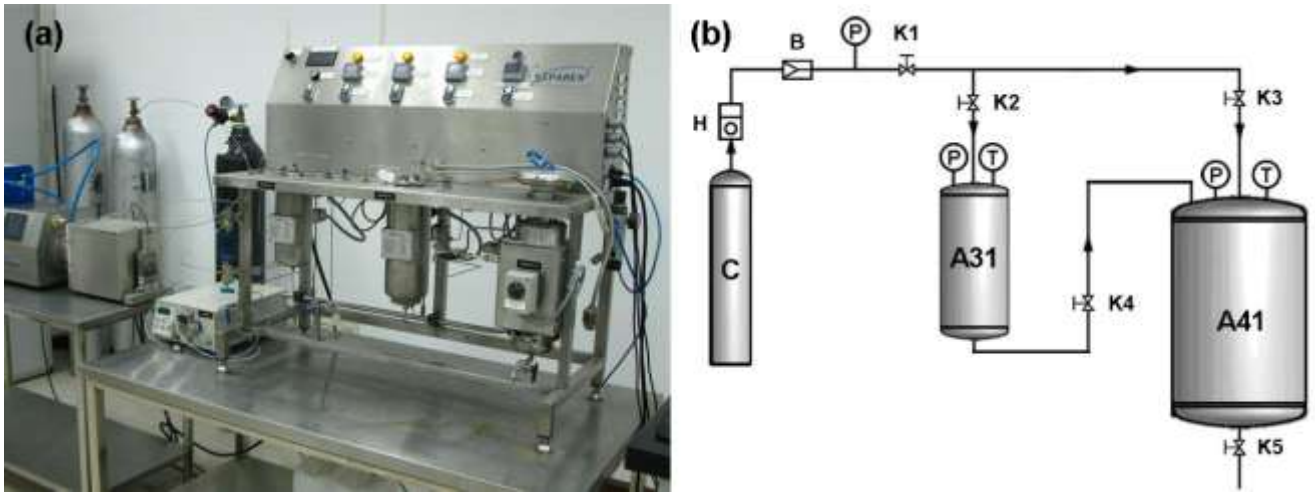

Fig. S1 The photograph (a) and schematic drawing (b) of supercritical fluids experimental apparatus. C: CO_2 Vessel, H: circulating cooler, B: pressure pump, P: pressure gauge, T: temperature gauge, K1~K5: valve, A31: reactor with heater, A41: reactor with heater and stirrer.

Fig. S1a showed that the multi-functional supercritical fluids experimental equipment was manufactured by SEPAREX S.A. (France). The CO_2 gas with high purity (99.999%) was supplied by Shanghai Pujiang Special Gas Co., Ltd (China). The technics flow shown in the figure (S1b) was designed for synthesizing the nanomaterials. The samples were synthesized as the following method. The key parts of experimental apparatus were the two reactors of A31 and A41 with heater and stirrer. The valves were used for controlling the flow of SC-CO_2.

In a typical procedure, 5.0g Zinc nitrate hexahydrate ($Zn(NO_3)_2 \cdot 6H_2O$) was dissovled into 20 ml deionized water. After stirring for a short time the resulting transparent solution was transferred into the reactor A41. Then the reactor A41 was heated to 120 ^oC for 24 h in the $ScCO_2$ pressure of 200 bar. Then the powdery sample was obtained and directly dried by $ScCO_2$ fluid and CO_2 gas stream. Before characterazations the as-prepared sample was collected from K5 and calcined at 200 ^oC, 400 ^oC and 600 ^oC for 2 h in air.

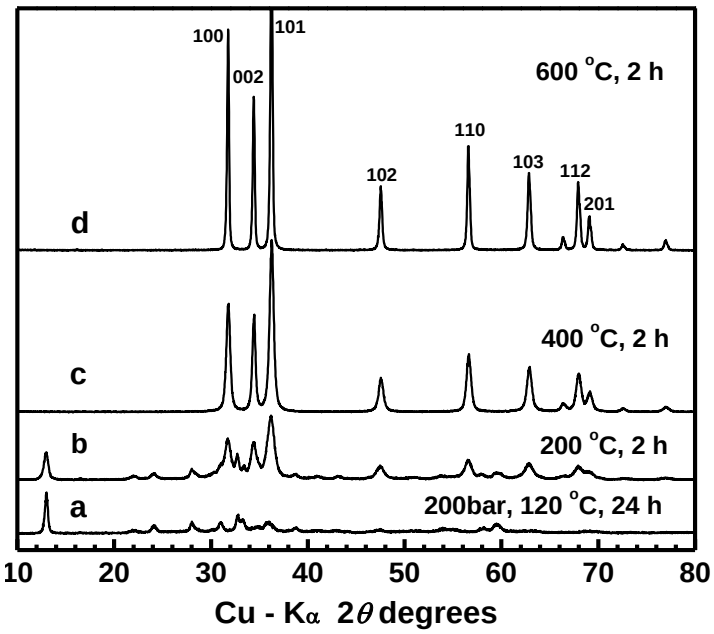

Fig. S2 XRD patterns of the samples obtained under supercritical CO_2 assisted solvothermal treatment at 200 bar, 120 °C for 24 h (a), and obtained by calcining the as-prepared sample above for 2 h at 200 °C (b), 400 °C (c) and 600 °C (d), respectively.

Crystallographic and purity information were obtained using powder XRD. To analyze these materials, the samples were after centrifugation and later air-dried upon deposition onto glass slides. Diffraction patterns of these materials were collected using a powder diffractometer (RIGAKU D/max-2600/PC) operating in the reflection mode with CuKα radiation at a scan rate of 0.02 ° $2\theta \cdot s^{-1}$.

Crystalline informations of sample obtained under supercritical CO_2 assisted solvothermal treatment is shown in Fig. S2a. The diffraction peaks of as-produced sample at $2\theta \approx 13.0$ °, 28.2 °, 32.7 ° correspond well with the (200), (020), (021) lattice planes of hydrozincite, which is a kind of basic zinc carbonate with the formula of $Zn_5(CO_3)_2(OH)_6$ (JCPDS 19-1458). Fig. S2b gives the XRD diffraction pattern of the sample was calcined at 200 °C for 2 h, which shows that several new diffraction peaks emerged at $2\theta \approx 31.8$ °, 34.4 °, 36.3 ° correspond well with the (100), (002), (101) lattice planes of Zincite ZnO (JCPDS 36-1451). In addition, the diffraction peaks assigned to $Zn_5(CO_3)_2(OH)_6$ shown if Fig. S2b is weaker than that of peaks Fig. S2a, indicating the intermediate of phase transition from $Zn_5(CO_3)_2(OH)_6$ to ZnO. Both Fig. S2c and S2d give typical XRD patterns of Zincite ZnO (JCPDS 36-1451) calcined at 400 °C and 600 °C for 2 h, respectively. Moreover, diffraction peaks assigned to Zincite ZnO shown in Figs. S2b-S2d are intensified step by step with the increasing of calcined temperatures, indicating the crystalline growth of ZnO nanoparticles with the elevation of calcined temperatures after the accomplishment of phase transition from $Zn_5(CO_3)_2(OH)_6$ to ZnO.

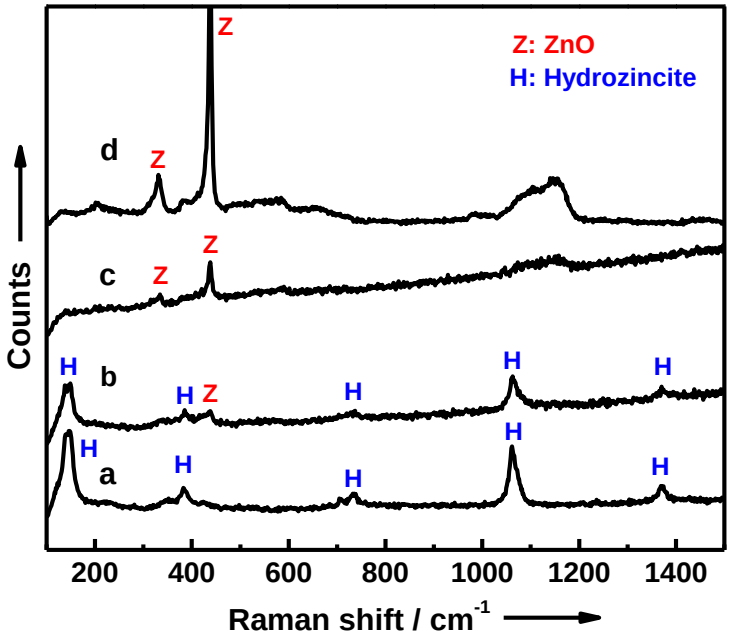

Fig. S3 Raman spectras for the samples obtained under supercritical CO_2 assisted solvothermal treatment at 200 bar, 120 ^oC for 24 h (a), and obtained by calcining the as-prepared sample above for 2 h at 200 ^oC (b), 400 ^oC (c) and 600 ^oC (d), respectively.

Raman spectra analysis was conducted on the samples using a Renishaw inVia+Reflex spectrometer and an excitation wavelength of 785 nm with incident power of 30 mW. The laser power was kept low enough to avoid heating of the samples by optical filtering and/or defocusing the laser beam at the sample surface. Spectra were collected in the range of 1500-100 cm^{-1} with a resolution of 1 cm^{-1}.

The samples were investigated by Raman spectroscopy (Fig. S3). Fig. S3a shows the peaks at about 148, 382, 736, 1061 and 1369 cm^{-1} should be assigned to hydrozincite $Zn_5(CO_3)_2(OH)_6$ without contamination.[1-3] Fig. S3b gives the Raman band of the sample was calcined at 200 ^oC for 2 h, which shows that the new peak emerged at 438 cm^{-1} should be assigned to E_2(high) mode of Zincite ZnO, indicating the intermediate stage of phase transition from $Zn_5(CO_3)_2(OH)_6$ to ZnO. Figs. S3a and S3b exhibit the obvious peaks at about 331 and 438 cm^{-1} can be assigned to $3E_{2H}-E_{2L}$ multiphonon vibration and E_2(high) mode of Zincite ZnO without contaminations, respectively.[4-5] Moreover, the Raman peaks assigned to Zincite ZnO shown in Figs. S3b-S3d are intensified step by step with the increasing of calcined temperatures. Therefore, the Raman spectras for the samples shown in Fig. S3 indicate the phase transition from $Zn_5(CO_3)_2(OH)_6$ to ZnO and the crystalline growth of ZnO nanoparticles with the elevation of calcined temperatures, which correspond well with the XRD results shown in Fig. S2.

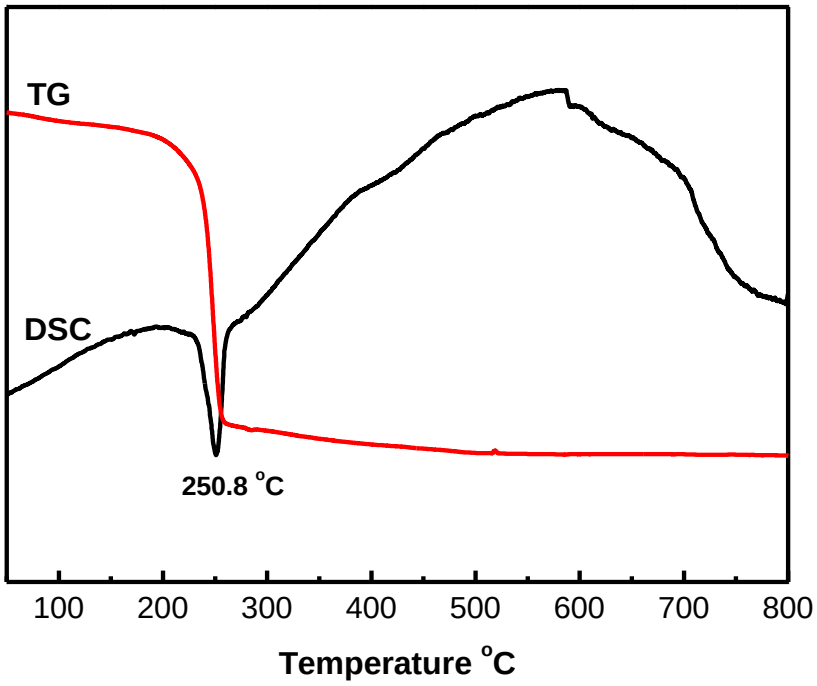

Fig. S4 TG-DSC diagrams for the sample obtained under supercritical CO_2 assisted solvothermal treatment at 200 bar, 120 °C for 24 h.

The dehydration and transformation behaviors of the as-prepared hydrozincite $Zn_5(CO_3)_2(OH)_6$ were analyzed by thermogravimetry-differential thermal analysis (Linseis STA PT1600) in the range 20-800 °C at a heating rate of 10 °C min^{-1}.

A TG-DSC analysis was carried out to investigate the thermal conversion characteristics of the as-prepared hydrozincite $Zn_5(CO_3)_2(OH)_6$. Fig. S4 shows an endothermic peak centered at around 250.8 °C in DSC curve and the weight loss of 24.89 % in TG curve, which should be probably attributed to the decomposition of $Zn_5(CO_3)_2(OH)_6$ by release of water and carbon dioxide. [6, 7] The endothermic peak centered at around 250.8 °C is less than that of endothermic peak reported in the literature (281 °C [8]). The as-prepared product of hydrozincite $Zn_5(CO_3)_2(OH)_6$ obtained under supercritical CO_2 assisted solvothermal treatment without contamination of any organic residues [8] may be the probable reason why the phase transition from hydrozincite $Zn_5(CO_3)_2(OH)_6$ to ZnO occurs in a lower temperature.

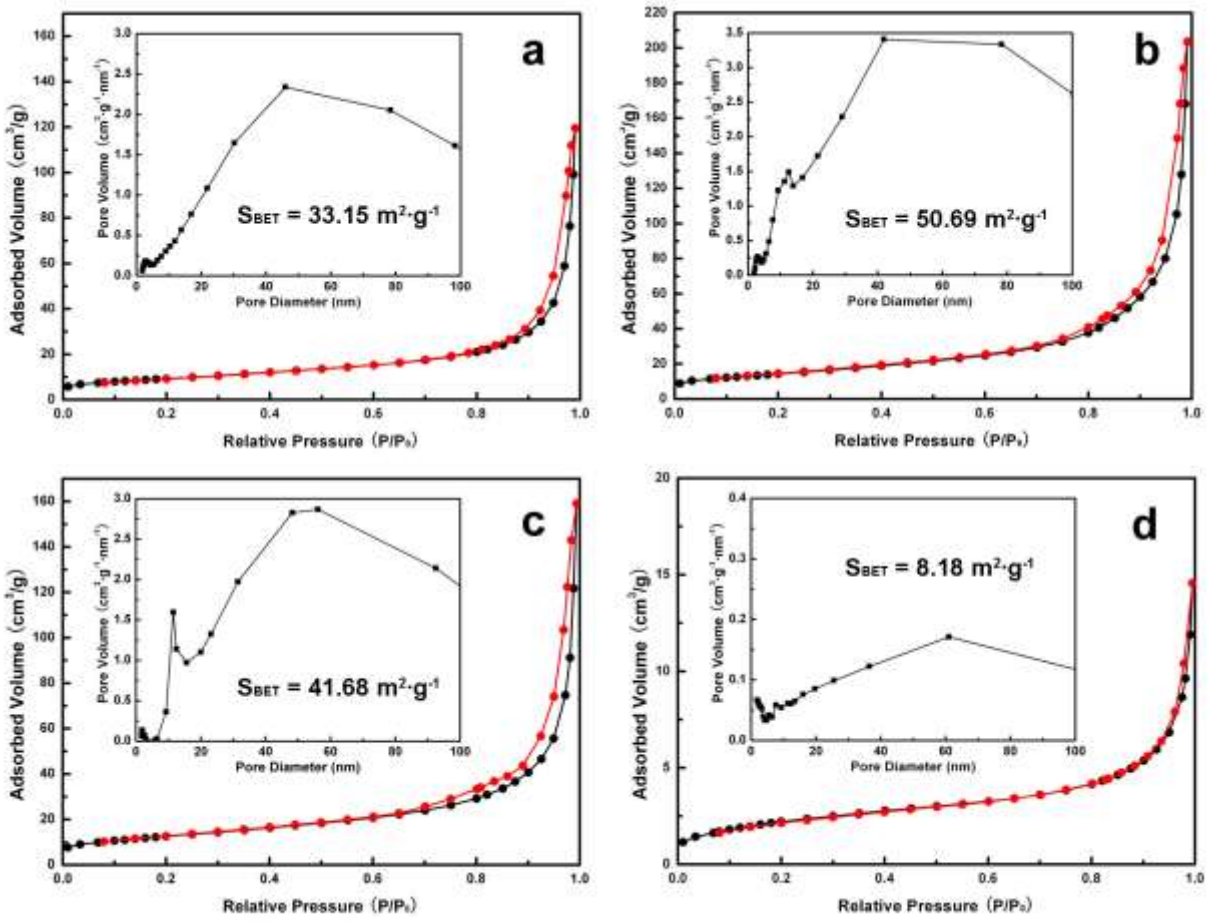

Fig. S5 N_2 adsorption/desorption isotherms and pore size distributions for the samples obtained under supercritical CO_2 assisted solvothermal treatment at 200 bar, 120 ^oC for 24 h (a), and obtained by calcining the as-prepared sample above for 2 h at 200 ^oC (b), 400 ^oC (c) and 600 ^oC (d), respectively.

Specific surface areas were measured by Nitrogen adsorption-desorption method using ASAP 2020 Micromeritics apparatus following the BET analysis. Adsorption and desorption of N_2 were performed at -196 ^oC. Samples had been previously outgassed by heating at 100 ^oC under vacuum (3 mm Hg). Desorption isotherm was used to determine the pore size distribution using the Barret-Joyner-Halender (BJH) method.

Fig. S5 gives the N_2 adsorption-desorption isotherms and Barret-Joyner-Halenda (BJH) pore size distribution plots (insets) of the products. It is also clear that the uncalcined sample (Fig. S5a, inset) contained a somewhat greater proportion of large macropores with diameters > 20 nm, which should be produced by the unique morphologies of nanosheets assembled $Zn_5(CO_3)_2(OH)_6$ nanoflowers. The pore size distribution of the calcined product obtained at 200 ^oC (Fig. S5b, inset) exhibits not only a broad porous distribution with diameters > 20 nm but also a weak mesoporous peak centered at about 12 nm. A large amount of vacancies should be formed accompanied by the formations of new Zn-O bonds as the result of the generations of CO_2 and H_2O and escaped from the crystalline structure of $Zn_5(CO_3)_2(OH)_6$, and the expansion of vacancies may result in the formation of cracks and mesoporous holes at the nanosheets in the phase transition proces. Therefore, this weak peak is probably assigned to the cracks and a small amount of mesoporous holes at the nanosheets in the phase transition proces. Consequently, the pore size

distribution of the calcined product obtained at 400 ^{o}C (Fig. S5c, inset) exhibits not only a broad porous distribution with diameters > 20 nm but also an obvious narrow mesoporous peak centered at about 12 nm, which should be assigned to the mesoporous holes at the nanosheets as well as the formation of hierarchically structured ZnO nanomaterial with flower-sheet-particle mophologies. When the the as-prepared product is heated to 400 ^{o}C, the cracks are further expanded and the ZnO nanoparticles with more distinct profiles are formed. Therefore, this obvious stronger peak is probably assigned to the large amount of mesopores at the nanosheets accumulated by ZnO nanoparticles. Finally, the pore size distribution of the calcined product obtained at 600 ^{o}C (Fig. S5d, inset) exhibits a very weak porous distribution, which correspond well with the collapse of the hierarchical ZnO structure. Meanwhile, the S_{BET} specific surface areas of the uncalcined product, calcined product obtained at 200, 400 and 600 ^{o}C are 33.15, 50.69, 41.68 and 8.18 $m^2 \cdot g^{-1}$, respectively. The S_{BET} specific surface areas increase firstly and then decreases with the increment of calcination temperatures, indicating the formtion of cracks at the nanosheets in the phase transtion process and then the crystal growth of ZnO nanoparticles at higher temperatures. In addition, the Brunauer–Emmett–Teller (BET) and Barrett–Joyner–Halenda (BJH) analysis correspond well with the results of SEM characterizations.

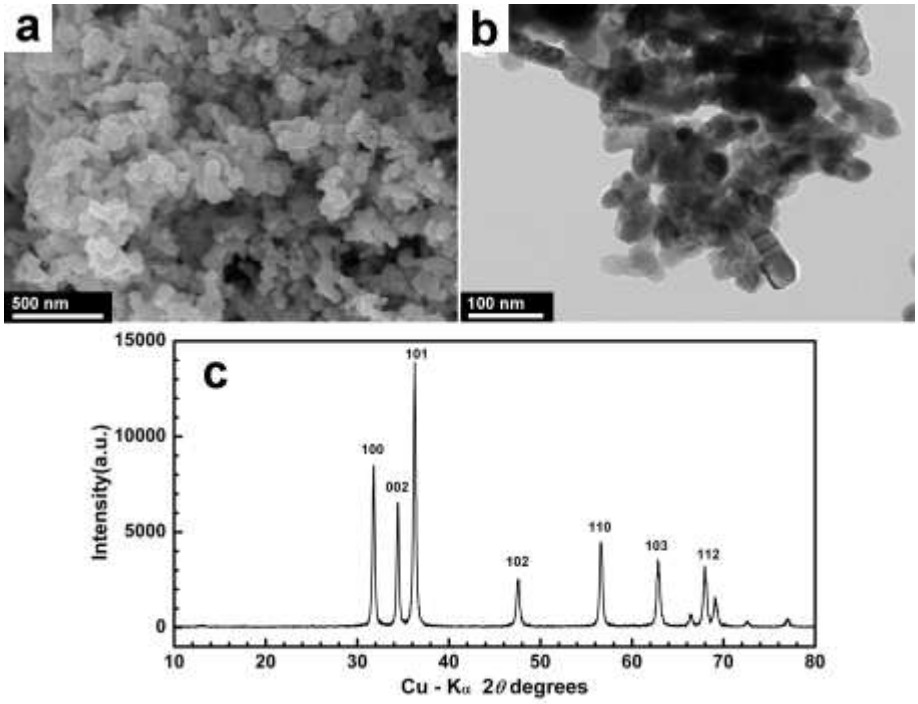

Fig. S6 SEM (a), TEM (b) images and XRD pattern (c) of commercial ZnO nanoparticles.

A comparative experiment was schemed to evaluate the photocatalytic activity of hierarchically structured ZnO nanomaterials with flower-sheet-particle mophologies. The commercial ZnO nanoparticles was purchased from Aladdin Reagent (Shanghai) Co., Ltd with an average particle size of 30±10 nm, and the corresponding SEM, TEM images and XRD pattern were shown in Fig. S6, indicating that the commercial ZnO nanoparticles had a similar particle size to the product of hierarchically structured ZnO nanomaterials obtained at 400 ^{o}C. Fig. 4 shown in the text indicated that the hierarchically structured ZnO nanomaterials with flower-sheet-particle mophologies obtained at 400 ^{o}C exhibited the highest photoactivities in this work and obviously higher than that of the commercial ZnO nanoparticles (Aladdin Reagent, 30±10 nm) under identical conditions.

References

[1] C. H. Matthew and L. F. Ray, *Polyhedron*, 2007, **26**, 4955-4962.

[2] M. Bucca, M. Dietzel, J. Tang, A. Leis and S. J. Köhler, *Chem. Geol.*, 2009, **266**, 143-156.

[3] L. Y. Yang, G. P. Feng and T. X. Wang, *Mater. Lett.*, 2010, **64**, 1647-1649.

[4] Q. Deng, X. Duan, D. H. L. Ng, H. Tang, Y. Yang, M. Kong, Z. Wu, W. Cai and G. Wang, *ACS Appl. Mater. Inter.*, 2012, **4**, 6030-6037.

[5] X. Wang, Q. Zhang, Q. Wan, G. Dai, C. Zhou and B. Zou, *J. Phys. Chem. C*, 2011, **115**, 2769-2775.

[6] F. Zhou, Z. L. Hu, Y. Q. Fan, S. Chen, W. P. Ding and N. P. Xu, *J. Phys. Chem. C*, 2008, **112**, 11722-11728.

[7] H. Jing and J. H. Zhan, *Adv. Mater.*, 2008, **20**, 4547-4551.

[8] S. Liu, C. Li, J. Yu and Q. Xiang, *CrystEngComm*, 2011, **13**, 2533-2541.